Final Draft
of the original manuscript:

Schulz-Stellenfleth, J.; Stanev, E.V.:
Statistical assessment of ocean observing networks – A study of water level measurements in the German Bight
In: Ocean Modelling (2010) Elsevier

DOI: 10.1016/j.ocemod.2010.03.001

Statistical assessment of ocean observing networks - A study of water level measurements in the German Bight

J. Schulz-Stellenfleth, E.V. Stanev

GKSS Research Centre (GKSS), Institute for Coastal Research, Max-Planck Str. 1, D-21502 Geesthacht, Germany, Tel: +49 (0)4152 87 1511, Fax: +49 (0)4152 87 1565

Abstract

A set of tools for the statistical assessment of ocean observing networks is presented and applied for the analysis of different instrumentation scenarios in the German Bight. An optimal linear estimator is used to re-construct ocean state parameters from observations taking into account both the prior distribution of the state and measurement errors. The proposed method enables a re-construction of any scalar parameter or vector field with linear relationship to the state. The performance of the observing network is quantified in terms of the re-construction quality. Apart from the capability of the network to provide estimates of state parameters at the time of the observations, the potential of the measurements for forecasts is investigated as well. Furthermore a generic method to compare single measurements with continuous observations is presented. Finally a technique is described to quantify the relative importance of different components of an observational network.

The proposed methods are applied to water level measurements in the German Bight. A numerical model is used to estimate the background statistics. Synthetic measurements provided by tide gauges, satellite altimeters, and HF radar are considered in the analysis. The estimation of the complete water level field in the German Bight is compared for altimeter and tide gauge measurements. It is shown that the orientation of the satellite track with respect to the coastline is of high relevance. The importance of water level measurements taken in deeper water, e.g., at the FINO-1 platform, is demonstrated. It is shown that continuous tide gauge measurements provide

Email address: johannes.schulz-stellenfleth@gkss.de (J. Schulz-Stellenfleth, E.V. Stanev)

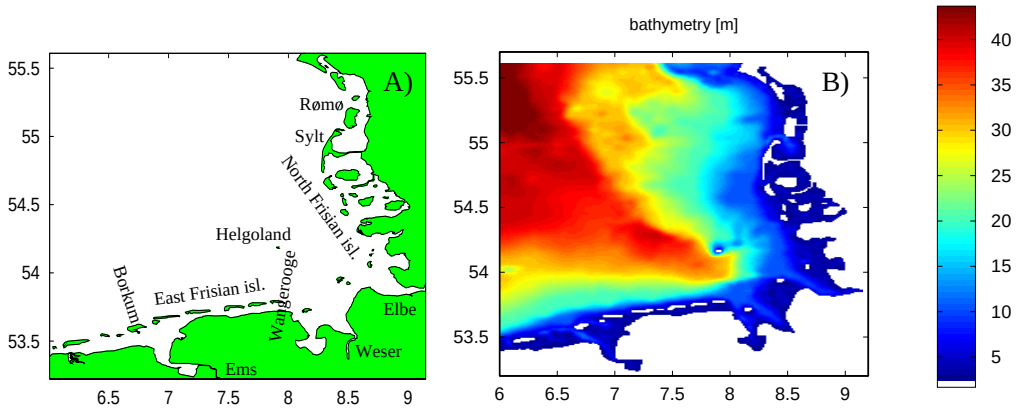

Figure 1: (A) Map of the German Bight. (B) Bathymetry of the German Bight.

more information on the area mean water level in the German Bight than altimeter observations taken by ENVISAT and JASON-1/2. It is furthermore shown how the information provided by a tide gauge propagates with the Kelvin wave. Implications for the design of an assimilation scheme are discussed.

Key words: performance assessment, tide gauges, radar, ocean tides, ocean circulation, sensitivity analysis

1. Introduction

With the upcoming of new ocean observing instruments like gliders, FerryBox sensors (Petersen, 2006), or X-band radar (Robinson et al., 2008) a wealth of new information is becoming available about physical and biochemical processes in the sea. The optimal combination of new and existing instruments as well as their configuration requires tools and techniques to assess the performance of observing networks. This problem has been subject of several previous studies (Bretherton et al., 1976; Hackert et al., 1998; Sakov and Oke, 2008; Frolov et al., 2008; Le Hénaff et al., 2009). The assessment of the expected system performance is also a particularly critical issue for the planning of future satellite missions (Mourre et al., 2006b).

The most common applications of observational networks are monitoring of the ocean state, validation of numerical model simulations, and assimilation of data in numerical models. All these applications can have different

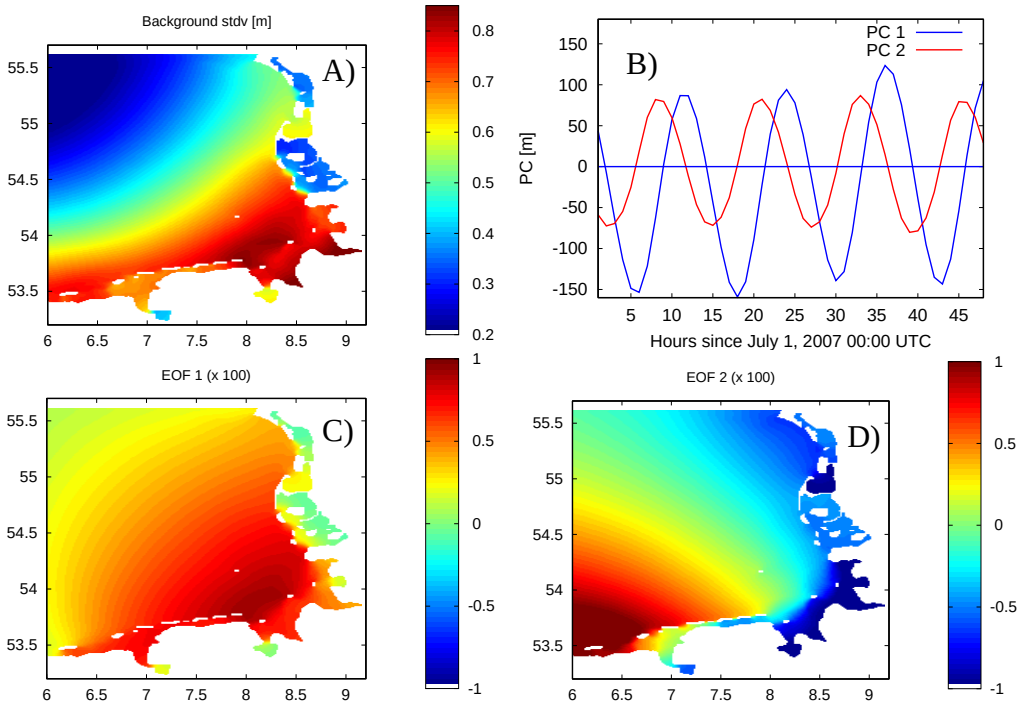

Figure 2: (A) Water level STDV derived from the numerical model for July 2007. (B) First two principal components for July 1/2, 2007 corresponding to the EOFs shown in (C) and (D). (C),(D): First two dominating EOF modes for July 2007.

requirements and very specific assessments have therefore been carried out e.g., in Mourre et al. (2006b). However taking into account that many networks are used for different applications there is a need to assess and optimise networks in a quite general sense. The perfect situation for all three applications mentioned above would be to have continuous measurements of all relevant variables. As this is in general not feasible the observations should at least be suitable to re-construct the desired quantities as accurate as possible. Different approaches have been presented to address this problem, most of which using a priori information about the background statistics of the ocean state. For example Le Hénaff et al. (2009) proposed the representer matrix spectra method, in which patterns in observation space are identified, which can be measured by the network particularly well. Another approach, e.g., taken by Frolov et al. (2008) is based on the optimal linear estimation of the ocean state from given measurements. The performance of the network

is then quantified in terms of the respective estimation errors. The present study follows the second approach and was guided by the following three questions. (1) How well can we re-construct the ocean state from measurements ? (2) How much information do measurements give us about future states ? (3) Which components of the network are important ? The first and second question are strongly connected to the data assimilation problem; in the context of data assimilation the measurements should contain information required to identify and correct forecast errors. Such observations can then be used in the analysis to improve the initial fields for the next forecast step.

In this study several components are added to the existing technical framework for observation network assessments. The main technical contributions of the paper are as follows.

- A weighting matrix is introduced, which allows to assess a network with regard to the estimation of different quantities, which can be chosen according to specific applications.
- An approach to obtain a first order assessment of forecast capabilities of a network is presented.
- A simple approach to compare single measurements and continuous observations is introduced.
- The relative importance of different sensors of an observational network is quantified based on a sensitivity analysis.

The methods are applied to water level measurements in the German Bight. Tide gauges, satellite altimeters, and ground-based radar systems operating in the high frequency regime (HF radar) are considered. The re-construction of different scalar parameters and vector fields is demonstrated. In particular the complete water level field for the German Bight is estimated from tide gauge and altimeter data. Altimeter and tide gauge measurements are also assessed concerning their ability to provide information on the spatially averaged water level. The ability of observing networks to capture certain dynamical patterns is studied by re-construction of principal components associated with empirical orthogonal functions (EOFs) of the water level.

The propagation and dispersion of the information gathered by an observational network is an important issue for the design of assimilation systems.

In particular for the choice of the assimilation interval an analysis of the respective behaviour is important. In this study we present a simple approach for this purpose, which is based on a statistical forecast. The method is applied to tide gauge measurements in the German Bight. The role of the coastal wave in the information propagation is discussed.

Comparisons of the impact of satellite altimeter systems and tide gauges have been performed in previous studies using sophisticated assimilation systems (Mourre et al., 2006b). In this study we present a simple method to compare continuous tide gauge measurements and single snapshot observations as provided by satellite altimeters. The information gathered by both systems over a certain period is quantified in terms of bits. The statistical forecast method mentioned above is used to estimate the loss of information over time for tide gauge measurements.

Finally the importance of the accuracy of different tide gauges and altimeter measurements is analysed. This is of relevance for the extension of existing networks with additional sensors or the replacement of an existing sensor by a more precise instrument.

In the state re-constructions presented in this paper we use the background covariance matrix as a priori information and thus the network is assessed in terms of its ability to capture the natural variability of the system. If we assume that the model forecast errors have a similar covariance structure as the background statistics the re-construction capability of a network also says something about the ability to improve the initial state needed for a forecast in an assimilation environment. In case the forecast errors have a different structure than the background statistics, the methods in this paper can still be used to assess the usefulness of the observations for assimilation by simply replacing the background covariance matrix by the forecast error covariance matrix.

The study is performed as part of the German project COSYNA (Coastal Observation System for Northern and Arctic seas), which aims at optimising the data exploitation of observational networks in the North Sea and further develop coastal ocean forecasting capabilities.

The paper is structured as follows: Section 2 describes the general dynamics of the relevant North Sea variables, as well as the numerical model used to estimate the respective covariance statistics. Section 3 is about the basic properties of the measurement instruments used in the study. Section 4 introduces the basic elements of a statistical approach to assess observational networks by analysis of re-construction errors. In section 5 the basic

elements of the method are applied to compare altimeter observations and tide gauge measurements. Section 6 is about the signal to noise ratio (SNR) of re-constructed scalar parameters. An assessment of different HF radar configurations is presented in section 7. Section 8 introduces a method to assess networks based on statistical forecasts. This method is then used in section 9 to compare single snapshot measurements as, e.g., taken by satellite altimeters with continuous observations. Finally section 10 describes a method to quantify the relative importance of different components of an observational network.

2. Model set up

The German Bight considered in this study is part of the North Sea, which is dominated by tides with a typical tidal range of 2-4 m and a dominant period of 12.4 hrs. The largest non-tidal variations are caused by atmospheric low pressure systems, either as external surges from the North Atlantic or internally generated surges. During strong storm events water levels can exceed 4 m above mean sea level. The German Bight is furthermore characterised by very shallow water with Wadden Sea areas falling dry during low tide. In this study the 3-D numerical model GETM (Burchard and Bolding, 2002) is used to simulate the hydrodynamical processes in the German Bight. A map of the German Bight and the bathymetry of the 203 km by 258 km model domain is shown in Fig. 1 (A) and (B) respectively. GETM is a primitive equation model, in which the equations for the three velocity components and sea surface height, as well as the equations for turbulent kinetic energy and the eddy dissipation rate are solved. The application of the model to the area of our study is described in Staneva et al. (2009). The model is run on a spherical grid with 1 km resolution. Terrain following equidistant coordinates (σ-coordinates) are used for the vertical dimension. The water column is discretised into 21 nonintersecting layers. The model is forced by 1) atmospheric fluxes estimated by the bulk formula using 6-hourly ECMWF re-analysis data (wind, atmospheric temperature, relative humidity and cloud cover) and simulated by the model SST, 2) hourly river run-off data provided by the Bundesamt fur Seeschifffahrt und Hydrographie (BSH), and time varying lateral boundary conditions of sea surface elevations and salinity. The sea surface elevations of the open boundary are generated using simulated data from a larger-scale model for the North Sea and Baltic Sea with coarser resolution (about 5 km). This model uses the same computa-

tional code (GETM). The sea surface elevation at the open boundary of the North Sea-Baltic Sea model is generated using tidal constituents. Temperature and salinity at the open boundary are interpolated from monthly mean climatological data described in Janssen et al. (1999).

The agreement between observations and simulations demonstrated in Staneva et al. (2009) proves that the model simulates the basic dynamics and thermodynamics. Fig. 2 (A) shows the distribution of water level standard deviations for July 2007. The absolute standard deviation (STDV) is 0.538 m in this case. The water level dynamics is dominated by the passage of a 12.4 hr period Kelvin wave propagating from the west to the north east. It takes about 5 hrs for the wave to cross the model domain. The wave is circulating around an amphidrome, which is about 1 deg west of the model domains north west corner. Strong variations of the water level dynamics near the coast are associated with the complicated bathymetry in those shallow areas. Fig. 2 (C) and (D) show the first two dominating empirical orthogonal functions (EOFs), which explain 97.8 % of the water level dynamics in the German Bight. The first EOF corresponds to sea level variations with uniform sign and a maximum in the Elbe estuary. The second EOF has alternating sign and describes back and forth motions of the sea level. The corresponding principal components (PCs) for July 1/2, 2009 are shown in Fig. 2 (B). As one can see the second mode follows the first mode with about 90° phase shift. Both modes together capture most of the water level dynamics associated with the coastal wave.

In the following analysis the elevations as well as the zonal and meridional surface current components in all permanently flooded grid points are used. The number of these wet points is $n_w = 37997$. The dimension of the state vector used for the analysis of water level fields in sections 5 and 6 is $n = n_w$. With the additional use of surface current fields in section 7 the dimension becomes $n = 3\,n_w = 113991$. The statistical analysis is based on hourly model output for July 2007. In particular the EOFs used to approximate the state covariance matrix were estimated from that period.

3. Synthetic Observations

In this section the measurement instruments used in the subsequent analysis are introduced. The relationships between the observations and state variables of the numerical model are described. Furthermore information is

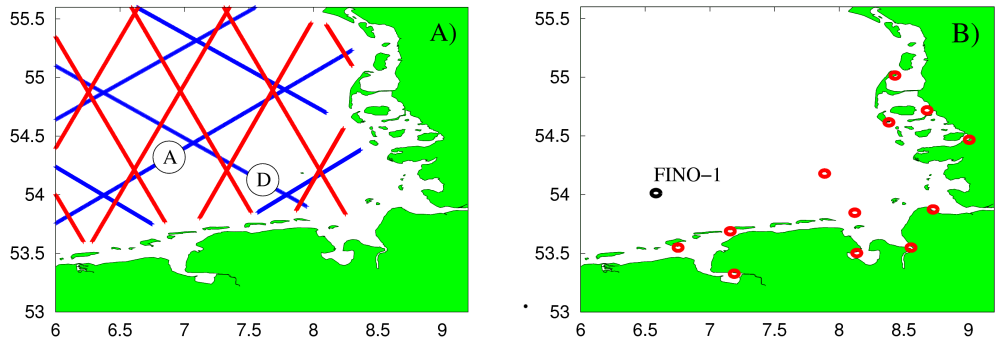

Figure 3: (A) Ground tracks of the altimeter satellites Jason-1, Jason-2 (blue) and ENVISAT (red).(B) Positions of 13 tide gauges used in the analysis (red: coastal and island stations, black: offshore platform station).

given on measurement errors. The general configuration of the instruments is chosen to be as close as possible to existing sensors.

3.1. Tide gauges

Tide gauge measurements are an important component in the validation and assimilation of ocean circulation models (Mourre et al., 2006a). In this study a network of 13 tide gauges as depicted in Fig. 3 (B) is investigated. Six of the gauges are located on islands (Borkum, Norderney, Wittdün, Helgoland, Lighthouse "Alte Weser", List on Sylt), four are situated in the three major river estuaries (Emden, Wilhelmshaven, Bremerhaven, Cuxhaven) and the remaining two (Husum, Dagebüll) are installed in small mainland harbours. These tide gauges represent a subset of a larger amount of available instruments, which are regarded as particularly reliable (Jensen and Mudersbach, 2004). As an option we will discuss the additional use of water level measurements at the FINO-1 platform about 45 km north of the island Borkum.

A measurement error of 0.05 m was assumed for all tide gauges. A discussion of the various error sources for tide gauge measurements can, e.g., be found in Soerensen and Madsen (2004).

3.2. Satellite Altimeter

A spaceborne radar altimeter is a nadir looking active microwave sensor. The signal round-trip time and the electromagnetic propagation speed are

used to estimate the distance from the antenna to the sea surface. Satellite altimeters such TOPEX/Poseidon, ERS-1/2, GFO, ENVISAT or JASON-1/2 have been successfully used to study large scale ocean circulation phenomena. Because of a number of technical problems these instruments were until a few years ago only rarely used for coastal regions however. With the standard processing techniques the data quality within 50 km from the coast was poor. With the development of more precise instruments and processing methods the application of radar instruments in coastal areas seems to be have become more feasible (Mourre et al., 2006b; Anzenhofer et al., 1999).

The altimeter measurements are affected by different error sources such as system noise, ionospheric delays, wet and dry tropospheric delays, electromagnetic bias and orbit uncertainties. In this study an accuracy of 4 cm is assumed for an instantaneous measurement of the JASON-1/2 and ENVISAT altimeters (Fu and Cazenave, 2000; Mourre et al., 2006b). The footprint of the sensor depends on sea state and is typically 3-5 km. Measurements are typically provided with 1 Hz sampling which corresponds to 6 km along track spacing. With this acquisition period we assume the measurement errors to be independent. The exact repeat cycle of the instrument depends on the satellite orbit and is 10 days for JASON-1/2 and 30 days for ENVISAT.

One revolution of the JASON-1/2 platforms takes 6745 s and two subsequent orbits are separated by 28° in longitude. Fig. 3 (A) shows the tracks of the JASON-1 and JASON-2 satellites in blue and the ENVISAT track in red. The tracks of JASON-1 refer to the orbit flown since Feb 2009. Following Mourre et al. (2006b) we disregard altimeter measurements within the 15 km littoral band to account for the data processing problems, which still exist near the coast (Anzenhofer et al., 1999). One ascending and one descending track labelled with "A" and "D" will be analysed in more detail in the following sections.

3.3. HF radar

High-frequency radar systems can provide continuous two dimensional current measurements over an area approaching 10000 km^2. The HF radar measurements provide information on velocities of the surface layer and represent averages over typically 1 km^2. HF radars like WERA (Gurgel et al., 1999) have been installed at different sites in the German Bight, e.g., St. Peter Ording (Essen et al., 1981; Barth et al., 2010), Sylt (Essen et al., 1984), Büsum, Helgoland (Essen et al., 1981; Barth et al., 2010), and Wangerooge (Schlick et al., 1990).

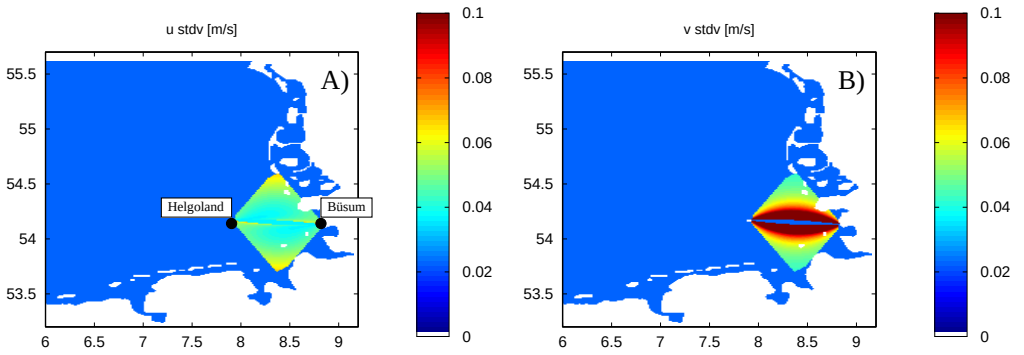

Figure 4: HF radar measurement errors for the zonal (A) and the meridional (B) current components. Two radar stations located at Büsum and Helgoland are assumed to provide radial velocities with an error of 0.05 m/s.

Following Breivik and Saetra (2001) we assume σ_{hf}=5 cm/s error standard deviation for the radial velocity component. The resulting errors for the u and v current components estimated from a system with two radar stations follow from straightforward geometric considerations. This issue is often referred to as geometric delusion of precision (GDOP) in literature (Chapman et al., 1997). For each point in the area covered by the two radar stations a matrix

$$A_{hf} = \begin{pmatrix} \xi_1 \\ \xi_2 \end{pmatrix} \tag{1}$$

is defined, where ξ_1, ξ_2 are row vectors of unit length pointing from the respective antenna positions to the considered location. The error covariance matrix G_{uv} for the u and v current components is then given by

$$G_{uv} \;=\; A_{hf}^{-1}\, G_{hf}\, \left(A_{hf}^{-1}\right)^T \,, \tag{2}$$

where $G_{hf} = \sigma_{hf}^2\, I_2$ is the error covariance matrix of the radial components measured by the two stations and I_2 denotes the 2 by 2 identity matrix. A singular value decomposition technique is applied to the cases with near singular matrix A_{hf}.

Fig. 4 shows measurement errors for the zonal (A) and meridional (B) current component for a system with two stations located at Büsum and Helgoland looking to the west and east. The blue coloured area in Fig. 4 (B) between the two antennas indicates points, for which the meridional current component was not estimated due to singularities of the matrix A_{hf}.

4. State Re-construction

The core part of the network assessment approach taken here follows standard methods in estimation theory. Similar techniques have in fact been used in the context of ocean observing networks before (Bretherton et al., 1976; Frolov et al., 2008). The analysis is furthermore strongly linked to the standard Kalman filter theory used in data assimilation (Robinson et al., 1998; Bennett, 1992). To have a clear foundation for the presentation of the new aspects we will start with an introduction of the basic elements of the approach.

Let x denote the state vector of the circulation model with dimension n. In the following it is assumed that the state vector x has the temporal mean removed. The observations are given by an observation operator H which maps x onto a measurement vector y of dimension m. Assuming that the mapping process is linear with y describing departures from the temporal mean in measurement space we can write

$$y = Hx + \epsilon \tag{3}$$

with a $m \times n$ matrix H and zero mean measurement noise ϵ, which we assume to be Gaussian. Let's furthermore denote the prior covariance matrix of the state vector by P and the measurement error covariance matrix by G. The state vector dynamics and the measurement noise are assumed to be statistically independent. In the following we will estimate the state x from a given measurement y using a linear approach, i.e.,

$$x = Ky \tag{4}$$

with a re-construction matrix K. A reasonable approach is to choose K such that the re-construction error (RE) is as small as possible. To derive such a matrix we define

$$d = x - K\left(Hx + \epsilon\right) = (I - KH)x - K\epsilon \ , \tag{5}$$

which is the difference between the true state x and the state estimated from a noisy measurement using an inversion matrix K. The absolute RE is then defined as

$$\rho_{ar}^{W} = \langle d^T W^T W d \rangle^{0.5} \ . \tag{6}$$

Here, $\langle \cdot \rangle$ denotes the averaging operator. Furthermore, we have introduced a matrix W, which can be used to weight and select different components.

Depending on the dimension of W the re-construction of both scalar quantities and vectors with linear relationship to the state x can be analysed. We will discuss different choices of W at the end of this section.

Using some general rules about the expectation value of quadratic forms and defining $Q = I - KH$ we find

$$\begin{aligned} \rho_{ar}^{W} &= \langle x^T Q^T W^T W Q x + \epsilon^T K^T W^T W K \epsilon \rangle^{0.5} \\ &= tr(WQPQ^T W^T + WK\, GK^T W^T)^{0.5} \quad , \end{aligned} \tag{7}$$

where tr denotes the trace of a matrix. To find a matrix K, which minimises the absolute RE we take the derivative of the square of eq. 7 resulting in

$$\frac{\partial (\rho_{ar}^{W})^2}{\partial K} = 2\, W^T W \left(-PH^T + KHPH^T + KG\right) . \tag{8}$$

The gradient is zero if we choose

$$K = PH^T B^{-1} \quad , \tag{9}$$

where we have assumed that the matrix B defined as

$$B = HPH^T + G \tag{10}$$

is invertible. The matrix K is the well known Kalman gain matrix, which plays a major role in data assimilation (Bennett, 1992; Brasseur, 2006; Robinson et al., 1998). The optimal re-construction can be interpreted as an analysis with no information from the forecast, i.e., the mean state is taken as the a priori state estimate.

In case B is singular we get an infinite number of solutions for K (with the same RE). This can happen if the observation network contains redundant measurements. One can then pick out one special solution, e.g., by singular value decomposition, i.e.,

$$B = V_B \lambda_B V_B^T . \tag{11}$$

We then replace B^{-1} by $V_B \hat{\lambda}_B^{-1} V_B^T$, where $\hat{\lambda}_B^{-1}$ contains the inverse eigenvalues and zeros for eigenvalues close or equal to zero.

With the particular form of the matrix K given by eq. 9 the expression for the RE eq. 7 simplifies to the posterior error

$$\rho_{ar}^{W} = tr\big(W^T W (P - PH^T B^{-1} HP)\big)^{1/2} . \tag{12}$$

Eq. 9 shows different behaviours of K. First of all, if the measurement error is big (i.e. $G \to \infty$) K tends to zero. This makes sense, because in this case the mean model state ($x = 0$) is the best state estimate. The same happens if $G \neq 0$ and $P \to 0$, because the model signal will be drowned in the measurement noise in this case as well. If there is no measurement noise, i.e., $G = 0$ one finds that the re-constructed state exactly reproduces the measurement, i.e., $H\,x = y$. This can be verified by setting $W = H$ in eq. 12. It is also interesting to note that the solution for K does not depend on the weighting matrix W. This means that, if the objective was to optimise the re-construction at a certain location or of a certain EOF mode, the re-construction matrix K would still provide a best estimator.

To reduce the dimension of the problem it can be reasonable to express the state in terms of EOFs (Lermusiaux, 1999). Denoting the EOF decomposition of the model error covariance matrix P by

$$P = VUV^T \tag{13}$$

the model state x can be expressed as

$$x = V\alpha \tag{14}$$

with a vector of expansion coefficients α. The re-construction matrix for the EOF coefficients is then given by

$$K_\alpha = V^T\,K = UV^T H^T B^{-1}\,. \tag{15}$$

In cases where the dynamics is dominated by a few EOFs it makes sense to perform the re-construction with a reduced rank approximation of P with a dimension of α much smaller than n. In this study the first 50 EOFs estimated from model results for Jul 2007 (compare section 2) were used for the analysis. These modes represent the temporal variability of the state variables on time scales between 1 hour and 1 month. The remaining EOFs contribute less than 0.0001 % to the water level variance. The EOFs were estimated using the "dual" approach (Preisendorfer, 1988). Here, a singular value decomposition is applied to a squared matrix, with dimension equal to the number of available time steps, which is 744 in our case. In particular it is not necessary to compute the complete state covariance matrix of dimension n by n.

As pointed out before there are alternative ways to choose P, e.g., based on an ensemble of model runs generated by perturbation of uncertain parameters or forcing fields (Mourre et al., 2004). In this case P represents model

RE	TG_{12}	TG_{13}	ALT_A	ALT_D
ρ_{ar}^{rms}	0.066 m	0.048 m	0.071 m	0.187 m
ρ_{rr}^{rms}	12.32 %	8.89 %	13.12 %	34.79 %
ρ_{ar}^{obs}	0.037 m	0.037 m	0.013 m	0.014 m
ρ_{rr}^{obs}	5.84 %	5.90 %	2.57 %	2.72 %

Table 1: Different re-construction errors (REs) for two tide gauge networks and two altimeter tracks (see text for details).

forecast errors. The methodology described in the present study could be applied the same way for such a choice of P. The interpretation and results would be different however, because the respective assessments would refer to the ability of observing networks to detect certain model errors and not to capture the temporal variability.

To relate the RE to the background variance associated with the ocean dynamics we define the respective relative error as

$$\rho_{rr}^{W} = \frac{\rho_{ar}^{W}}{\sqrt{tr(WPW^T)}} \cdot 100\% \, . \tag{16}$$

In simple words the relative error is the percentage of the background variability of the quantity Wx, which is not captured by the measurements.

5. Comparison of tide gauge networks and altimeter tracks

In the following we will evaluate eq. 12 and eq. 16 with different choices of the matrix W to compare tide gauge networks and altimeter tracks in the German Bight. To quantify the re-construction quality for the entire state it is natural to define W as

$$W = W_{rms} = n^{-1/2} \, I_n \tag{17}$$

with the $n \times n$ identity matrix I_n. With this choice $\rho_{ar}^{W} = \rho_{ar}^{rms}$ is the global root mean square (rms) error.

It may also be of interest to analyse the re-constructed state only at the observation points. This is achieved by defining W as

$$W = W_{obs} = m^{-1/2} \, H \tag{18}$$

with the measurement operator H. In this case $\rho_{ar}^{W} = \rho_{ar}^{obs}$ is the root mean square error at the measurement locations.

The re-construction was computed with a state vector containing the elevation field of dimension $n = 37997$ as described in section 2 and measurement errors defined in section 3. A nearest neighbour approach was used to define the measurement operator H, i.e., for a certain measurement location the matrix element corresponding to the grid point closest to this position was set to one and the remaining elements were set to zero.

Table 1 compares the absolute and relative RE for the following four observation scenarios:

- TG_{12}: Network of 12 tide gauges as indicated by the red circles in Fig. 3 (B).
- TG_{13}: The same as TG_{12}, but with one additional tide gauge at the FINO-1 platform (black circle in Fig. 3 (B)).
- ALT_A: The ascending JASON-1 track labelled with "A" in Fig. 3 (A).
- ALT_D: The descending JASON-1 track labelled with "D" in Fig. 3 (A).

One can see from table 1 that the network TG_{13} gives the best overall re-construction quality. Comparing TG_{12} and TG_{13} it is also evident that the inclusion of a tide gauge at the FINO-1 location leads to a significant improvement of the global re-construction.

For the altimeter one can see that the descending track gives global REs more than twice as big as the ascending track. We will analyse the origin of this behaviour in section 5.1.

For the RE at the observation points it is interesting to note that the altimeter tracks give values almost three times smaller than the tide gauges although the measurement errors for both instruments only deviate by 20 % (compare section 3). This behaviour can be explained by the fact that the distance of the altimeter footprints is much smaller than the distance of the tide gauges. In particular the gap between two altimeter footprints is smaller than the correlation length of the water level elevation field. The re-construction procedure can make use of this fact by averaging the measurement noise of subsequent altimeter observations leading to relatively small REs.

To give an impression about the distribution of REs a Monte Carlo simulation with 5000 realisations was carried out. An ensemble of elevation fields

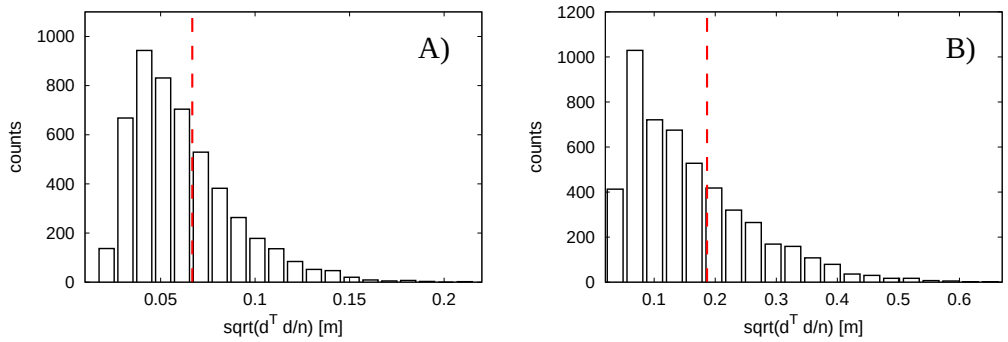

Figure 5: (A) Histogram of REs estimated from 5000 Monte Carlo simulations for the tide gauge network TG_{12} (see text for details). The red dashed line indicates the mean. (B) The same for the descending altimeter track ALT_D.

in accordance with the covariance matrix P (compare section 4) was generated by linear combination of the first 50 EOFs. A random generator was used to produce the respective coefficients with the variances given by the corresponding eigenvalues (see eq. 13). Measurements were then simulated by applying the measurement operator H and by adding measurement noise (see eq. 3). Histograms of the global rms error $(d^T d/n)^{0.5}$ are shown in Fig. 5 for TG_{12} (A) and ALT_D (B). The dashed red lines indicate the mean values estimated from the sample, which deviate by less than 1% from the theoretical expectation values given by eq. 12. There are of course various methods to compare the two distributions, e.g., by analysis of percentiles or higher moments. The comparison of the expectation values used in this study is a natural approach that we believe to be reasonable for most applications.

5.1. Spatial distribution of REs

For the planning or extension of an observational network it is interesting to investigate the spatial distribution of the REs. The covariance matrix of the error vector d (see eq. 5) is given by

$$\langle d\, d^T \rangle = QPQ^T + KGK^T \quad . \tag{19}$$

For the particular choice of K given by eq. 9 this simplifies to

$$\langle d\, d^T \rangle = P - PH^T B^{-1} HP \ , \tag{20}$$

which is the so called posterior error covariance matrix. The diagonal of this matrix gives valuable information about the spatial distribution of the rms

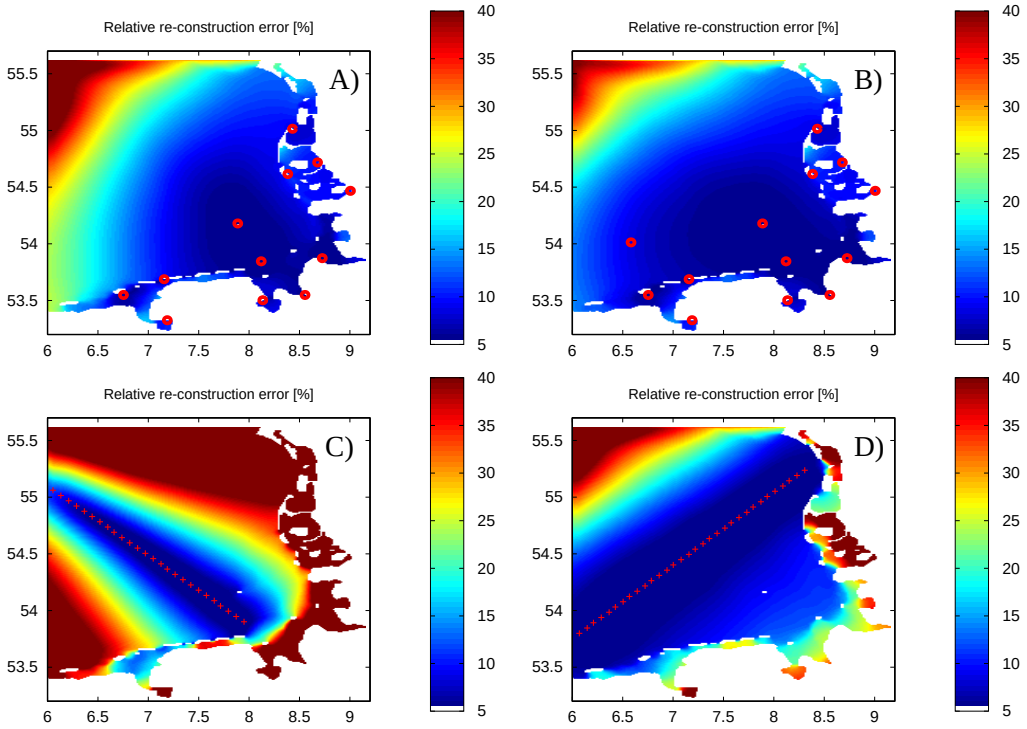

Figure 6: Relative water level REs for the tide gauge networks TG_{12} (A) and TG_{13} (B). (C,D) The same for the descending JASON-1 track ALT_D (C) and the ascending track ALT_A (D).

REs. In the following the spatial distribution of the relative error given by the n-dimensional vector

$$\rho_{rr}^{X} = 100\,\% \cdot \sqrt{\frac{\mathrm{diag}(\langle d_X d_X^T \rangle)}{\mathrm{diag}(P)}} \tag{21}$$

is discussed for the different sensors introduced in section 3.

The spatial distribution of REs obtained from the tide gauge array TG_{12} is shown in Fig. 6 (A). One can see that the errors are increasing in the north west direction, which is reasonable, because of the large distance from the measurements. Slightly increased ($> 10\%$) RE are are also found in the Ems estuary, the East Frisian Wadden Sea and the Wadden sea area south of the island Sylt. This was to be expected, because the dynamics in these shallow water areas is particularly complex (Stanev et al., 2007). It is also evident that the information gathered by the most westerly tide gauge in the

		TG_{12}	TG_{13}	ALT_A	ALT_D
Entire domain	ρ_{ar}^{mean}	0.038 m	0.025 m	0.019 m	0.066 m
	SNR^{mean}	10.3 dB	12.0 dB	13.2 dB	7.9 dB
Shallow water	ρ_{ar}^{mean}	0.019 m	0.019 m	0.059 m	0.188 m
	SNR^{mean}	14.0 dB	14.1 dB	9.1 dB	4.1 dB

Table 2: Absolute REs and SNRs for the mean water level estimated from two different tide gauge networks and two altimeter tracks for the entire domain and shallow water (depth < 10 m).

semi-enclosed area behind the island Borkum is not spread northwards into the open sea.

Fig. 6 (B) shows the corresponding REs for the extended network TG_{13}. One can see that the FINO-1 tide gauge leads to a significant improvement in the south westerly part of the domain. This demonstrates the importance of having tide gauges in the open part of the shelf area in addition to measurements in the semi-enclosed areas along the coast.

The respective REs for a descending and ascending JASON-1 altimeter track are given in Fig.6 (C) and (D) respectively. One can see that the ascending track gives much better re-constructions of the water levels than the descending track. This is because the ascending track is more or less perpendicular to the crest of the Kelvin wave (see Fig. 2 (D)). As the highest correlations of the water levels are naturally found along the crests of the wave this configuration gives an optimal spread of information to both sides of the satellite track.

6. SNR of scalar parameters

In this section the re-construction of scalar parameters computed from the state according to

$$\beta = \zeta^T x \tag{22}$$

with a column vector ζ of dimension n is investigated. To compute the estimation error for such parameters we evaluate eq. 7 with a single row matrix W^ζ defined as

$$W = W^\zeta = \zeta^T \, . \tag{23}$$

The absolute re-construction error for the parameter β can then be expressed as

$$\rho_{ar}^\zeta = \left(\zeta^T (QPQ^T + KGK^T)\, \zeta\right)^{1/2} \, . \tag{24}$$

The variance of β associated with the ocean dynamics is given by $\zeta^T P \zeta$. To relate the RE to this "signal" we define the SNR of β as

$$SNR_\beta = \frac{\sqrt{\zeta^T P \zeta}}{\rho_{ar}^{\zeta}} \quad . \tag{25}$$

The SNR is commonly used in the context of signal processing and is usually expressed in terms of dB (i.e. $10 \log_{10}(\cdot)$). For example 0 dB (or less) means that the ocean signal is drowned in the RE, i.e., the measurement is of no use in this case. A value of 3 dB means that the measurement is sufficient to determine at least the sign of the ocean signal.

6.1. Re-construction of the mean

One scalar parameter that maybe of interest is the mean of all state components. The respective RE can be computed by choosing

$$W = W^{mean} = n^{-1} \, (1, \ldots, 1) \, , \tag{26}$$

where n is the state dimension. In our case this choice provides a re-construction of the area mean water level in the German Bight. The absolute REs and SNR values obtained with the 4 instrumentation scenarios introduced in section 5 are summarised in table 2. Both the entire domain and the shallow water area with water depth below 10 m were considered. For the entire domain we see that the ascending altimeter track ALT_A gives the best result. Both tide gauge networks perform better than the descending altimeter track. One can also see that the inclusion of the FINO-1 observation leads to a significant improvement of the tide gauge network if the whole domain is considered. For the shallow water area both the TG_{12} and TG_{13} network perform better than the altimeter tracks. The difference between TG_{12} and TG_{13} is negligible in this case. The descending altimeter track hardly gives any useful information about the shallow water area.

6.2. Re-construction of PCs

Denoting by V_i the ith column of the matrix V (see eq. 13) we define the weighting matrix as

$$W = W_i^{EOF} = V_i^T \, . \tag{27}$$

With this choice of W the re-construction procedure provides an estimate of the principal component associated with the ith EOF of the state. Table 3

	C^i_{EOF}	TG_{12}	TG_{13}	ALT_A	ALT_D
EOF_1	70.97%	12.0 dB	13.5 dB	12.9 dB	9.0 dB
EOF_2	26.80%	8.7 dB	11.4 dB	10.2 dB	2.1 dB

Table 3: SNRs (given in dB) for the re-construction of the first 2 dominant EOFs (see text for details).

summarises the respective SNR values obtained for the re-construction of the first two dominant EOFs (compare Fig. 2 (C,D)). The second column gives the relative contribution of the EOF to the total variance. The remaining EOFs only contribute 2.2 % to the variability. Columns 3-6 give the respective SNR values for the two tide gauge arrays and the two altimeter tracks. One can see that the tide gauge network TG_{13} gives the best results for both EOFs. Concerning the first two EOFs the second best choice is the ascending altimeter track. As one can see the inclusion of the FINO-1 tide gauge has a particularly strong impact on the estimation of the second EOF.

6.3. Scaled Representers

The approach presented in Le Hénaff et al. (2009) is related to the analysis described in section 6.2. A fundamental difference is however that the investigation in Le Hénaff et al. (2009) is based on scalar parameters γ, which are not derived from the state x, but from the measurement y, i.e.,

$$\gamma = \xi^T y \tag{28}$$

with a vector of weighting coefficients ξ. The respective SNR is then given by

$$SNR_\gamma = \frac{\xi^T H P H^T \xi}{\xi^T G \xi} \; . \tag{29}$$

Assuming that G is nonsingular we may write $G = MM^T$, e.g., $M = G^{1/2}$ in the case where G is diagonal or by applying a Cholesky decomposition. It can be shown (McDonald, 1968) that the directions of the local maxima of eq. 29 are given by $\xi = (M^T)^{-1}\hat{\xi}$, where $\hat{\xi}$ are the eigenvectors of the matrix

$$C = M^{-1} H P H^T (M^T)^{-1} \; . \tag{30}$$

The maximum values are equal to the respective eigenvalues. In other words the dominant eigenvector of C defines the scalar parameter (see eq. 28) with the highest possible SNR. The matrix C is equal to the scaled representer

matrix defined in Le Hénaff et al. (2009). In that study the number of eigenvalues above unity is proposed as a measure of the observation network quality. If G is diagonal, nonsingular and homogeneous, i.e., $G = \sigma_y^2\, I$, the matrix of representers (Le Hénaff et al., 2009) is defined as

$$R = \sigma_y^{-1}\, P H^T V_C \;, \tag{31}$$

where the columns of V_C contain the eigenvectors of C. The columns of R represent directions in state space, which are mapped on the directions of high SNR values in measurement space as defined above. In that sense these states are characteristic for the observational network. The EOF analysis presented in section 6.2 goes in the opposite direction, because here the starting point is the dominant modes of the ocean system and the ability of observation network to detect these modes is used for the assessment.

7. HF Radar

As an example of sensors, which provide water level information in an indirect way we investigate in the following different configurations of HF radar systems.

As explained in section 3.3 HF radar systems measure the radial components of surface currents. To obtain information about the elevation from such measurements a state vector with dimension n=113991 consisting of the elevation field and the u and v surface current components is taken as input for the analysis described in section 4. The error model described in section 3.3 is used for the re-construction. Measurements were simulated on a regular grid with 3 km spacing within the area covered by the antennas. The measurement errors for each grid point were considered as independent. The resulting RE for the elevation field is shown in Fig. 7 (A). Here an HF radar system with two stations located at Büsum and Helgoland looking to the east and west respectively is considered. The relative rms RE obtained using a background covariance matrix estimated for Jul 2007 is 22.48 % in this case. One can see that the re-construction is reasonable, but worse than the general results achieved with tide gauges and altimeter tracks. Only the descending altimeter track ALT_D has a higher RE. Particular problems are found concerning the propagation of the information into the North Frisian Wadden Sea area.

The moderate performance of the above elevation re-construction is not a surprise, as there is no direct physical relationship between water levels and

simultaneous surface current vectors. The re-construction is therefore dominated by the background statistics. As an alternative the same technique is applied again, but this time with the elevation η replaced by the elevation rate of change $\mathrm{d}\eta/\mathrm{d}t$. For this parameter there is a clear connection to the vertically averaged current field v_{av} following from the continuity equation with constant water density

$$\frac{\partial \eta}{\partial t} = -\nabla \cdot (H v_{av}) \,, \tag{32}$$

where H is the water depth. As the surface current field measured by the radar is strongly correlated with v_{av}, smaller re-construction errors are expected for $\mathrm{d}\eta/\mathrm{d}t$ than for η. Fig. 7 (B) shows the relative RE for $d\eta/dt$ using the same radar configuration as above. The relative RE is $\rho_{rr}^{rms} = 11.88\%$ in this case. Apart from the overall better re-construction one can see that the information spread into the North Frisian Wadden Sea area is much better than obtained with the former approach. Fig. 7 (C) shows a configuration with only one station at Büsum. With this single station only the radial current component can be measured as explained in section 3.3. The error of $\rho_{rr}^{rms} = 13.92\%$ derived for this configuration shows that the system with two stations leads to a slightly better estimation of the water level rate of change. At first sight it seems surprising that the system with two stations does not give significantly better results than the system with one station. One should take into account however that the range of current directions captured by the two configurations is about the same. The second antenna station provides additional information on the detailed spatial structure of the current directions, but in this case the correlation length of the current field seems to be so long that these additional measurements only lead to a small improvement of the re-construction. At this point it should be emphasized again that the assessment described here is in a statistical sense, i.e., for the detection of a specific small scale current feature the benefit of a second atennna can very well be significant.

The re-construction quality obtained with a system with two antennas located at the islands Wangerooge and Helgoland looking to the North and South is shown in Fig. 7 (D). The RE of ρ_{rr}=17.31% is significantly worse than the value obtained with the Helgoland-Büsum system in Fig. 7 (B).

In summary one can say that the proposed assessment methods are applicable to HF radar measurements. One should also say however that in a realistic scenario HF radar current measurements would be used directly for

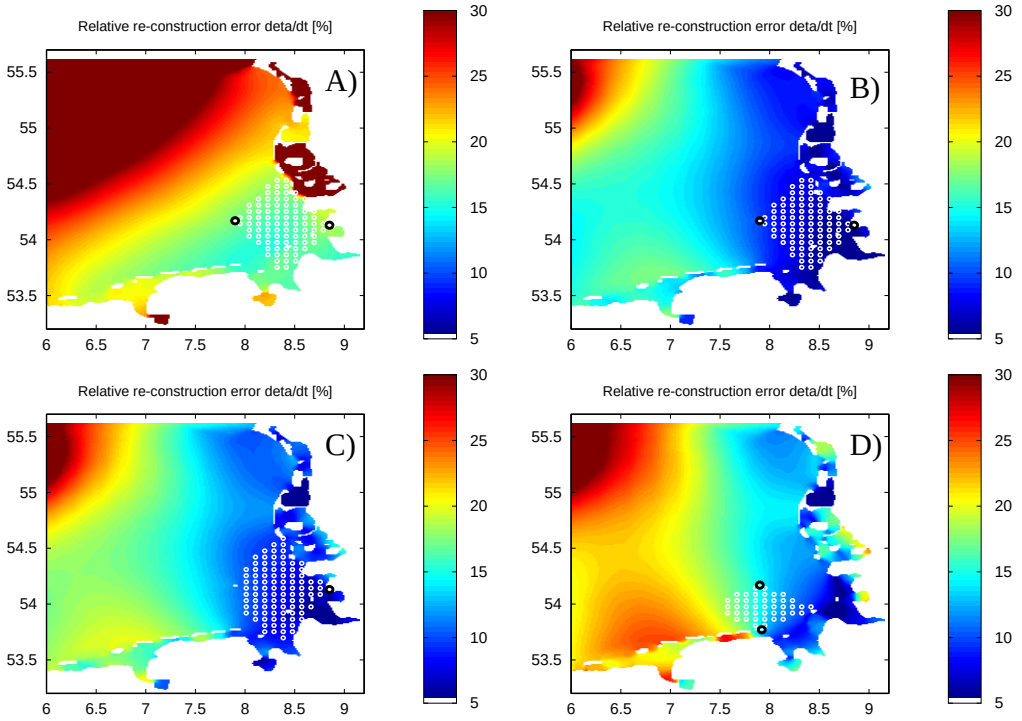

Figure 7: Relative REs obtained for Jul 2007 using different HF radar configurations. (A) Re-construction of the elevation η with two stations at Helgoland and Büsum. (B) The same as A), but for the elevation rate of change $\mathrm{d}\eta/\mathrm{dt}$. (C) The same as B), but with only one station at Büsum. (D) The same as B) but with two stations at Wangerooge and Helgoland.

the assimilation of a circulation model taking into account various nonlinear effects. The linear approach taken here can however still give a first idea about the information and the impact to be expected from the data.

8. Statistical Forecast

The method described so far provides a re-construction of the state at the time the respective measurements are taken. For applications like forecast it may also be of interest to assess the observational network with regard to its re-construction capability for future states. A first order analysis in this direction can be easily included in the generic methodology introduced above. Lets assume we want to re-construct the state $x(t)$ at time t from

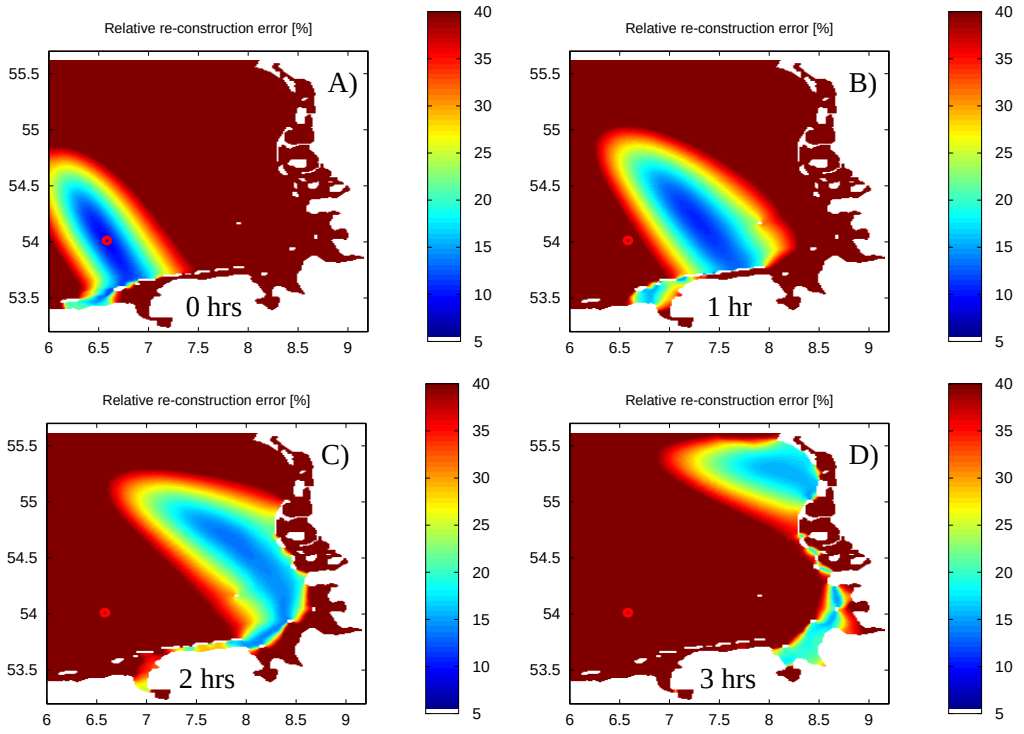

Figure 8: Relative REs obtained with a tide gauge at the FINO-1 research platform with time lags of 0 hr (A), 1 hr (B), 2 hrs (C), and 3 hrs (D).

measurements taken at $t - \Delta t$. We can then define an extended state vector

$$\hat{x}(t) = \big(x(t), x(t - \Delta t)\big) \tag{33}$$

and compute the covariance matrix $\hat{P}$ of the extended state as before (compare section 4). In practice one does not need the complete state $x(t - \Delta t)$, but just those components required to simulate the observations. For example for the tide gauge measurement discussed above we simply take

$$\hat{x}(t) = \big(x(t), Hx(t - \Delta t)\big) \tag{34}$$

with the measurement operator H. As we are interested in the RE for $x(t)$, we define the matrix W in eq. 6 as $W = C_{n,m}$ with a matrix $C_{n,m}$ defined as

$$C_{n,m} = \begin{pmatrix} I_n & Z_{n,m} \end{pmatrix}, \tag{35}$$

where $Z_{n,m}$ is an $n \times m$ matrix filled with zeros and I_n is the $n \times n$ identity matrix. Because we want to re-construct the state $x(t)$ based on measurements taken at $t - \Delta t$ we define the measurement operator for the extended state as

$$\hat{H} = \begin{pmatrix} Z_{m,n} & I_m \end{pmatrix} . \tag{36}$$

The re-construction for the state $x(t)$ is then given by

$$x(t) = C_{n,m}\, \hat{K}\, y(t - \Delta t) \ , \tag{37}$$

where $y(t - \Delta)$ denotes the measurements taken at $t - \Delta t$ and $\hat{K}$ is the gain matrix for the extended state computed as (compare eqs. 9,10)

$$\hat{K} = \hat{P}\, \hat{H}^T\, \hat{B}^{-1} \tag{38}$$

with $\hat{B}$ defined as

$$\hat{B} = \hat{H}\hat{P}\hat{H}^T + G \ . \tag{39}$$

Denoting the RE vector for the extended state vector by $\hat{d}$ (see eq. 5) the respective error for $x(t)$ is given by $d_{x(t)} = C_{n,m}\hat{d}$ and the corresponding error covariance matrix follows as (see eq. 20)

$$\langle d_{x(t)} d_{x(t)}^T \rangle = C_{n,m} \left(\hat{P} - \hat{P}\hat{H}^T \hat{B}^{-1} \hat{H} \hat{P} \right) C_{n,m}^T \ . \tag{40}$$

The method provides a forecast based on a pure statistical model. We therefore refer to these re-constructions as statistical forecasts.

To illustrate the technique Fig. 8 shows statistical forecast errors obtained from a single tide gauge at the location of the FINO-1 research platform. The relative errors are shown for time lags of 0 hrs (A), 1 hr (B), 2 hrs (C), and 3 hrs (D). One can clearly see how the information gathered by the tide gauge propagates with the Kelvin wave along the coast reaching the Elbe estuary after 2 hrs and leaving the model domain after about 4 hrs.

An analysis tool like this can help in the basic design and optimisation of an assimilation system. In particular the results can be used to choose suitable assimilation intervals. For example it makes sense to choose the period between two analysis time steps smaller than the time after which the area influenced by the measurement has left the model domain. On the other hand the assimilation intervals should be chosen long enough to ensure that a new measurement contains significantly more information than the previous observation. We will come back to this point in the next section.

Furthermore the instrument positions can be optimised for the forecast in a certain region and certain forecast intervals. For the water level in the German Bight we see that a measurement taken at the FINO-1 platform can be expected to have a positive impact on a 2 hours forecast for the Elbe estuary. One can also look at the limitations of observation networks concerning forecast improvements in a certain area. For example water level measurements in the German Bight can not be expected to have a significant impact on predictions in the same area if forecast periods longer than 4 hours are considered.

9. Continuous measurements

It is obvious that the ability of tide gauge networks or HF radars to provide continuous measurements is a big advantage compared to single snapshot measurements as, e.g., taken by satellite altimeters. To compare altimeter observations and tide gauge measurements one has to take into account two aspects:

- The number of independent measurements provided by each system.
- The information contained in each measurement.

For the first point it is essential to quantify the time gap, for which two measurements can be regarded as independent. In this study the method introduced in section 8 is used for this purpose. As explained before measurements provide a forecast capability with a certain time horizon. Lets assume a measurement has been taken at time t_0 and we ask after which time interval Δt a new measurement can be considered as independent. A straightforward approach is to compare the respective forecasts computed for the time $t_1 = t_0 + \Delta t$ with the re-construction obtained with a new measurement taken at t_1. The new measurement can be regarded as independent, if it contains significantly more information than already provided by the previous observation. We use a very simple approach and regard the difference as significant, if the RE for the forecast has exceeded the nowcast RE by a factor of two. One might also think of more sophisticated definitions, but for this study only a time scale is required and we will therefore not discuss this issue further.

Fig. 9 shows the normalised RE $\rho_{ne} = \rho_{rr}^{rms}(\Delta t)/\rho_{rr}^{rms}(0)$ for the tide gauge array TG_{12} as a function of the forecast horizon. Here, $\rho_{rr}^{rms}(\Delta t)$ denotes the

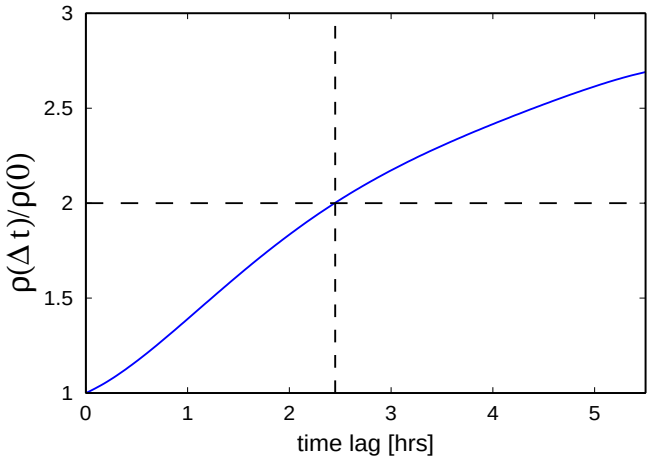

Figure 9: Normalised RE obtained with the tide gauge network TG_{12} for different time lags. The REs are divided by the respective value obtained for zero time lag.

rms RE obtained with the statistical forecast method described in section 8. As one can see the forecast error exceeds the nowcast error by a factor of two after approximately 2.5 hours. In the sense described above one can therefore say that within a Jason altimeter cycle of 10 days the tide gauge array TG_{12} acquires 96 independent measurements, while the altimeter only provides a single track.

On the other hand we have seen that for certain parameters like the mean water level the accuracy of this single altimeter measurement can be higher than the tide gauge observation. A simple approach to balance the observation accuracy and frequency requirements is to look at the respective information content (IC). The average information gain in terms of bits associated with a measurement can be expressed as (Tarantola, 1987)

$$IC = \int P_A^x \, \log_2 \, \frac{P_A^x}{P_B^x} \, dx \; , \tag{41}$$

where P_B^x and P_A^x are the probability distributions of the state before and after the measurement has been taken. In our case both distributions are Gaussian with zero mean. It is straightforward to show that the information gain for a scalar parameter β can then be expressed as (Tarantola, 1987)

$$IC_\beta = \log_2 SNR_\beta + \frac{1}{\ln 4}(SNR_\beta^{-2} - 1) \; , \tag{42}$$

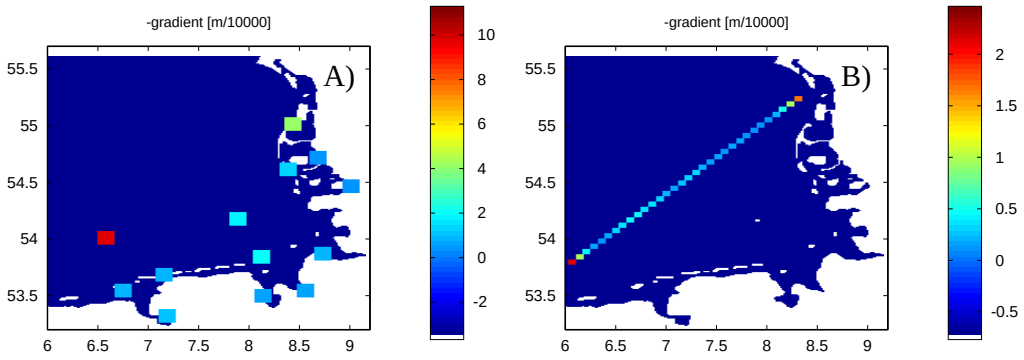

Figure 10: A) Gradient (sign inverted) of the squared rms re-construction error $(\rho_{ar}^{rms})^2$ with respect to measurement accuracies of tide gauges. B) The same for the accuracy of altimeter measurements.

where SNR_β was defined in eq. 25 and $\ln 4 \approx 1.39$ is calculated using the natural logarithm.

Using the above methodology the information gathered by tide gauges and altimeters was compared for a period of 30 days. Using results from section 6.1 we know that a single measurement with the TG_{12} tide gauge network provides 2.7 bits of information about the mean water level in the German Bight. Taking into account the correlation time discussed above this gives 777.6 bits of information for 30 days. The ENVISAT altimeter acquires 9 tracks in the German Bight within this period. Adding up the information contents for these tracks gives 15.6 bits. The JASON-1/2 altimeters provide 18 tracks within 30 days, giving another 32.2 bits. We see that with a total of 47.8 bits the altimeters provide about 6% of the information gathered by the tide gauge network.

Using an assimilation system for the North Sea Mourre et al. (2006b) also came to the conclusion that tide gauge measurements have a stronger impact than existing satellite altimeter systems at least within a coastal band of about 100 km width. Farther away from the coast satellite altimeters can complement tide gauge measurements very efficiently. It is also important to say that new altimeter systems providing better temporal sampling are at the horizon (Mourre et al., 2006b).

10. Sensitivity

In this section the relative importance of different sensors in the observational network is investigated. For this purpose the gradient of the RE eq. 12 with respect to parameters of the measurement operator H is computed. Lets assume H is a function of a parameter κ and $\partial H/\partial\kappa$ is the respective derivative. After some basic algebra the derivative of the RE with respect to κ is found to be

$$\frac{\partial(\rho_{ar}^{W})^2}{\partial\kappa} = -2\; tr\Big(B^{-1}HPW^TWP\,(I - H^TB^{-1}HP)\frac{\partial H^T}{\partial\kappa}\Big)\;. \qquad (43)$$

As a simple example we investigate the importance of the accuracy of different sensors. A straightforward approach would be to compute the derivative of eq. 12 with respect to the measurement error. We can also use eq. 43 however by scaling of the measured quantities with the measurement errors kept constant. To study the sensitivity of the RE with respect to the accuracy of the $\hat{k}$th sensor we therefore define $H(\kappa)$ as

$$H_{ij}(\kappa) = \begin{cases} \kappa\;\delta(j - j^*(\hat{k})) & \text{if } i = \hat{k} \\ \delta(j - j^*(i)) & \text{else}\;, \end{cases} \qquad (44)$$

where $j^*(i)$ denotes the position of the ith sensor. The derivative is then given by

$$\left(\frac{\partial H}{\partial\kappa}\right)_{ij} = \delta(i - \hat{k})\,\delta(j - j^*(\hat{k}))\;. \qquad (45)$$

For each instrument the derivative eq. 43 is computed in this way.

Fig. 10 (A) shows the resulting gradient with inverted sign for the tide gauge array TG_{13}. The rms error ρ_{ar}^{rms} was considered in this case (see eq. 17). One can see that the water level measurement at the FINO-1 platform is the most important one followed by the tide gauge located at the island of Sylt in the north. We have already seen in section 5.1 that the FINO-1 tide gauge is important, because due to local effects the Borkum tide gauge only provides limited information about the south western model domain. The tide gauge at Sylt seems to be of higher relevance, because the location is well suited to monitor the relatively strong tidal dynamics in the Sylt-Rømø Bay.

Fig. 10 (B) shows the same for the altimeter track ALT_A. Here one can see that the relative importance of the measurements taken at the beginning

and the end of the track is higher. This makes sense, because these measurements only have neighbouring observations on one side and are therefore less redundant than the measurements closer to the centre. Following the same arguments one can expect a general tendency of sensors at the boundary of observational networks to be relatively important. In practical terms this could mean that replacements of existing sensors by more accurate instruments should be done at the boundary first, because in many cases this will lead to the strongest improvement of the entire network performance.

11. Conclusions

The presented study was concerned with the assessment of ocean observing networks. The objective was to develop and test simple and robust methods to quantify the performance of such systems keeping in mind the variety of requirements encountered in practical applications.

An optimal linear estimator was used to re-construct parameters of interest from the observations using a priori information about the covariance structure of the ocean state vector. This basic approach follows methods introduced in previous studies and is strongly related to the Kalman filter used in sequential data assimilation methods. The present investigation adds several new aspects to the existing methodology. The estimation of scalar parameters was analysed using the SNR as a quality measure. In particular the detection of EOFs was discussed in this context. Furthermore a statistical forecast method was presented, which allows to analyse the propagation and dispersion of the information gathered by a measurement network. This approach was then used as part of a new technique to compare single measurements and continuous observations. Finally a method to quantify the relative importance of different components of an observational network was proposed.

The introduced methods were applied to synthetic water level measurements in the German Bight. Tide gauges, satellite altimeters and HF radar systems were investigated based on simulated observations. The performance of the altimeter was shown to be strongly dependent on the satellite heading with ascending paths giving better results. It was shown that under certain configurations altimeters can provide more accurate instantaneous estimates of the mean sea level than tide gauge arrays. However, because of the long repeat cycles of the existing satellite altimeters, tide gauges are able to provide more information, when periods of 10 days or longer are considered.

Furthermore it was shown that the tide gauge network gives more precise information about the shallow water areas than the altimeter.

It was furthermore demonstrated how the information gathered by tide gauges at the western boundary of the German Bight propagates with the Kelvin wave along the coast passing the Elbe estuary after 2 hours and leaving the northern boundary after about 4 hours. The implications for the use of tide gauge measurements in an assimilation system for the German Bight were discussed. In particular it was described how the analysis can help in a suitable choice of the assimilation interval.

Different configurations of HF radar systems with one and two antenna stations were used to estimate water levels and the respective rate of change. It was shown that the elevation change rate is easier to estimate than the elevation itself. It was furthermore demonstrated that the use of two stations at Büsum and Helgoland gives slightly better results than one station at Büsum and a significantly better performance than two stations located at Wangerooge and Helgoland.

Finally it was shown that water level measurements taken at the location of the FINO-1 platform are very beneficial. The use of this station has a particularly strong impact on the estimation of the second EOF. As a general finding it was furthermore concluded that there is a general tendency that observations taken at the boundary of observational networks are relatively important.

The presented methods will be further applied in the framework of the COSYNA project. In particular new data as, e.g., provided by gliders or the FerryBox system will be analysed. Furthermore the methods will be used in the context of data assimilation.

Acknowledgments

The study is performed as part of the German project COSYNA (Coastal Observation System for Northern and Arctic Seas), which aims at optimising the data exploitation of observational networks in the North Sea and further develop coastal ocean forecasting capabilities. Some parts of the present work have been stimulated and benefited by the research in the frame of the EU IP ECOOP on the synergy between new ocean observing instruments and numerical coastal forecasting. We thank both reviewers for their careful reading of the manuscript and many constructive hints and comments.

References

Anzenhofer, M., Shum, C., Rentsch, M., 1999. Coastal altimetry and applications. Technical Report. Ohio State University, Columbus, USA. No. 464, Geodetic Science and Surveying, 40 p.

Barth, A., Alvera-Azcárate, A., Gurgel, K.W., Staneva, J., Port, A., Beckers, J.M., Stanev, E., 2010. Ensemble perturbation smoother for optimizing tidal boundary conditions by assimilation of high-frequency radar surface currents - application to the German Bight. Ocean Science 6, 161–178.

Bennett, A., 1992. Inverse methods in physical oceanography. Cambridge University Press.

Brasseur, P., 2006. Ocean weather forecasting: An integrated view of oceanography. Springer. chapter Ocean data assimilation using sequential methods based on the Kalman Filter. pp. 271–316.

Breivik, O., Saetra, O., 2001. Real time assimilation of HF radar currents into a coastal ocean model. Journal of Marine Systems 28, 161–182.

Bretherton, F., Davis, R., Fandry, C., 1976. A technique for objective analysis and design of oceanographic experiments applied to mode-73. Deep-Sea Research 23, 559–582.

Burchard, H., Bolding, K., 2002. GETM - a General Estuarine Transport Model. Technical Report. European Comission. No EUR 20253 EN, printed in Italy.

Chapman, R., Shay, L., Graber, H., Edson, J., Karachintsev, A., Trump, C., Ross, D., 1997. On the accuracy of HF radar surface current measurements: Intercomparison with ship-based sensors. Journal of Geophys. Res. 102, 18737–18748.

Essen, H.H., Freygang, T., Gurgel, K.W., Schirmer, F., 1984. Oberflächenströmungen vor Sylt - Radarmessungen im Herbst 1983 -. Dt.hydrogr.Z. H.5, 201–215.

Essen, H.H., Mittelstaedt, E., Schirmer, F., 1981. On near-shore surface current measurements by means of radar. Ocean Dynamics 43, 1–14.

Frolov, S., Baptista, A., Wilkin, M., 2008. Optimizing fixed observational assets in a coastal observatory. Continental Shelf Research 28, 2644–2658.

Fu, L.L., Cazenave, A., 2000. Satellite altimetry and earth sciences: a handbook of techniques and applications. Academic Press.

Gurgel, K.W., Antonischki, G., Essen, H.H., Schlick, T., 1999. Wellen radar (WERA): a new ground wave HF radar for ocean remote sensing. Coastal Engineering 37, 219–134.

Hackert, E., Miller, R., Busalacchi, A., 1998. An optimized design for a moored instrument array in the tropical atlantic ocean. Journal of Geophys. Res. 103, 7491–7509.

Janssen, F., Schrum, C., Backhaus, J., 1999. A climatological data set of temperature and salinity for the Baltic Sea and the North Sea. Deutsche Hydrographische Zeitschrift Supp.9.

Jensen, J., Mudersbach, C., 2004. Zeitliche Änderungen in den Wasserstandszeitreihen an den Deutschen Küsten, in: Proccedings of the Workshop *Klimaänderung und Küstenschutz* at the University of Hamburg, pp. 115–128.

Le Hénaff, M., De Mey, P., Marsaleix, P., 2009. Assessment of observational networks with the representer matrix spectra method - application to a 3d coastal model of the Bay of Biscay. Ocean Dynamics DOI:10.1007/s10236-008-0144-7.

Lermusiaux, P., 1999. Data assimilation via error subspace statistical estimation, part ii: Middle atlantic bight shelfbreak front simulations and ESSE validation. Mon. Weather Rev. 127, 1408–1432.

McDonald, R.P., 1968. A unified treatment of the weighting problem. Psychometrika 33, 351–381.

Mourre, B., Crosnier, L., Le Provost, C., 2006a. Real-time sea-level gauge observations and operational oceanography. Phil. Trans. R. Soc. 364, 867–884.

Mourre, B., De Mey, P., Lyard, F., Le Provost, C., 2004. Assimilation of sea level data over continental shelves: an ensemble method for the exploration of model errors due to uncertainties in bathymetry. Dynamics of Atmosphere and Oceans 38, 93–121.

Mourre, B., De Mey, P., Menard, Y., Lyard, F., Le Provost, C., 2006b. Relative performance of future altimeter systems and tide gauges in constraining a model of North Sea high-frequency barotropic dynamics. Ocean Dynamics 56, 473–486.

Petersen, W., 2006. Ferrybox: A mature system for operational monitoring. Sea Technology 47, 53–57.

Preisendorfer, R., 1988. Principal Component Analyses in Metereology and Oceanography. Elsevier.

Robinson, A., Lermusiaux, P., Sloan, N., 1998. THE SEA: The Global Coastal Ocean: Processes and Methods. John Wiley and Sons, New York. chapter Data Assimilation. pp. 541–594.

Robinson, A., Lermusiaux, P., Sloan, N., 2008. Remote Sensing of the European Seas. Springer Netherlands, 2008. chapter Wave and Current Observations in European Waters by Ground-Based X-Band Radar. pp. 423–434.

Sakov, P., Oke, P., 2008. Objective array design: application to the tropical Indian Ocean. Journal of Atmospheric and Oceanic Technology 25, 794–807.

Schlick, T., Gurgel, K.W., Essen, H.H., Schirmer, F., 1990. Remotely controlled CODAR continouosly observed surface currents in the German Bight, in: Proccedings of the Fourth Working Conference on Current Measurements, pp. 15–21.

Soerensen, J., Madsen, H., 2004. Efficient Kalman filter techniques for the assimilation of tide gauge data in three-dimensional modeling of the North Sea and Baltic Sea system. Journal of Geophys. Res. 109.

Stanev, E., Flemming, B., Bartholomä, A., Staneva, J., Wolff, J.O., 2007. Vertical circulation in shallow tidal inlets and back-barrier basins. Continental Shelf Research 27, 798–831.

Staneva, J., Stanev, E., Wolff, J.O., Badewien, T.H., Reuter, R., Flemming, B., Bartholomae, A., Bolding, K., 2009. Hydrodynamics and sediment dynamics in the German Bight. a focus on observations and numerical modeling in the East Frisian Wadden Sea. Continental Shelf Research 29, 302–319.

Tarantola, A., 1987. Inverse Problem Theory. Elsevier Science.